Green Chemistry

Cutting-edge research for a greener sustainable future

Accepted Manuscript

Green Chemistry

Cutting-edge research for a greener sustainable future

rsc.li/greenchem

Volume 20
Number 9
7 May 2018
Pages 1919-2160

ISSN 1463-9262

ROYAL SOCIETY OF CHEMISTRY

PAPER
Paul T. Anastas *et al.*
The Green ChemisTREE: 20 years after taking root with the 12 principles

ROYAL SOCIETY OF CHEMISTRY

rsc.li/greenchem

Surface-functionalized mesoporous gallosilicate catalysts for the efficient and sustainable upgrading of glycerol to solketal

Alvise Vivian[1][#], Loraine Soumoy[1][#], Luca Fusaro[1], Sonia Fiorilli[2], Damien P. Debecker[3],*,
Carmela Aprile[1],*

[1]University of Namur, Department of Chemistry, Unit of Nanomaterials Chemistry, 5000 Namur, Belgium

[2]Department of Applied Science and Technology, Politecnico di Torino, Institute of Chemistry, 10129 Torino, Italy

[3]Université catholique de Louvain (UCLouvain), Institute of Condensed Matter and Nanosciences (IMCN), 1348 Louvain-la-Neuve, Belgium.

[#]These authors contributed equally to this work

*Corresponding authors: carmela.aprile@unamur.be ; damien.debecker@uclouvain.be

ABSTRACT

Two series of functionalized mesoporous Ga-silicates were prepared in a straightforward and sustainable one-pot procedure using different alkyl-silanes. The efficacy of the adopted co-synthetic approach based on aerosol processing has been proved by ^{29}Si solid-state NMR experiments revealing a degree of functionalization close to the theoretical value. The successful incorporation of gallium as single sites within the silica framework was confirmed via ^{71}Ga solid-state magic-angle-spinning NMR measurements.

These materials were tested as catalysts for the synthesis of solketal from glycerol at low temperature and under solventless conditions. A systematic study evidenced the importance of a careful tuning of surface polarity, achievable with surface functionalization as well as with different thermal treatments. The solids functionalized with a low degree of methyl groups (5%) displayed enhanced performances compared to the non-functionalized analogues, highlighting the highly beneficial role of surface hydrophobicity as well as the importance of the careful tuning of the hydrophilic/hydrophobic balance. The best functionalized catalysts proved to be easily reusable for multiple catalytic runs. With such high-performance catalyst in hands, we propose a process which show favorable E-factor, indicating that the production of solketal can be envisaged in a sustainable way.

Introduction

In 2015, the United Nations Member States adopted their "2030 Agenda for Sustainable Development", accelerating the transition toward, *inter alia*, more sustainable mobility and industry.[1, 2] In this context, the conversion of biomass into biofuels plays a pivotal role. Increasing the amount of biofuel in traditional fuels is now needed in order to fulfill the requirements of the European Commission: a minimum of 14% of renewable energy is required in road and rail transport by 2030.[3] On the biofuels market, biodiesel is gaining a growing importance due to its good compatibility with commercial diesel engines.[4] Nevertheless, its production via transesterification of triglycerides coming from natural lipid sources yields 10 wt.% of glycerol as by-product.[5] The more intense production of biodiesel over the last past years caused an oversupply of glycerol on the market.[6] Its price consequently suffered a drastic decrease and nowadays it is even considered as a waste. However, in the context of green chemistry, glycerol represents a very interesting building block as it directly comes from renewable feedstocks and can be produced via low energy consumption compared to petro-chemical based reagents.[7]

Glycerol offers a tremendous potential to produce value-added chemicals and the synthesis of solketal, through an acetalization reaction with acetone is a particularly relevant pathway.[8] On one side, solketal has various applications as solvent in large-scale productions (paint, ink formulations)[9], in the pharmaceutical industry (additive for injectables, vehicle for drug)[9] and even as fuel additive.[10, 11] The latter provides opportunities for the biorefineries to develop their circular economy. On the other side, this valorization pathway fulfills some of the 12 Principles of Green Chemistry established by Anastas and Warner[7]: glycerol and even acetone can be produced from renewable feedstocks (from triglycerides and hemicellulose,[13] respectively), the reaction can be classified as a high atom economy process (88%) and with a potential low E-factor.[12, 13]

Acetalization of glycerol is usually performed in the presence of homogeneous Brønsted or Lewis acid catalysts such as H_2SO_4, HCl, $SnCl_4$ or $Sn(OAc)_2$.[10, 14] Despite the high intrinsic activity of these homogeneous catalysts, scientists are working hard to develop heterogeneous catalysts, which can be recovered, reused or even implemented in continuous flow processes, thereby improving the sustainability of the process.[15] The use of zeolites, sulfonic acid functionalized silicates, K 10 montmorillonites, zirconia-based catalysts or gallo-silicates for the acetalization of glycerol has already shown promising results.[16-21] More recently, we proposed a new class of gallo-silicate catalysts synthesized via the aerosol-assisted sol-gel process, which show outstanding performances in the conversion of glycerol into solketal.[22]

In recent years, aerosol processes have emerged as efficient methods to synthesize heterogeneous catalysts displaying controlled properties for their application in a wide range of reactions.[23] For example, transition metal-doped silica and titania for oxidation of volatile organic compounds,[24] metal oxides for electrocatalysis,[25] titanosilicate catalysts for epoxidation,[26] or even supported metal nanoparticles for hydrogenation reactions[27] have

already been prepared by aerosol processes and shown excellent catalytic performances. In particular, the "aerosol-assisted sol-gel process" (AASG) emerged as an efficient tool to synthesize mesoporous silica-based solids featuring metal atoms inserted as single sites in their framework.[28] In this synthesis procedure, a sol containing a templating agent (e.g. a surfactant), solvent, silica and a metal precursors is nebulized into droplets that are gas-transported towards a drying chamber or tube, provoking the evaporation of the solvent. This fast evaporation triggers the self-assembly of the template used as sacrificial agent to generate pores and the rapid polycondensation of the inorganic precursors, yielding homogeneous materials with spherical shape. Compared to the traditional sol-gel route, the aerosol process presents several advantages including reduction of waste production, limited number of steps and low environmental impact. Moreover, the possibility to produce the solid in a continuous way makes it industrially attractive. [23, 29-31]

Regarding the conversion of glycerol into solketal, the development of highly performing heterogeneous catalysts has not yet been achieved. In order to design more efficient heterogeneous catalysts, it is well known that multiple characteristics can be optimized such as nature and number of active sites, mass transport of reactants and products to and from the active sites, surface area, pore size distribution, etc. However, an important and less studied parameter is the role played by the hydrophilic and hydrophobic properties of the catalyst surface. The latter influences strongly the adsorption of reagents and the desorption of products or by-products to/from the catalytic surface, thus determining the performances of the solid. Considering the mechanism of the acetalization of glycerol, the key role played by the hydrophilic and hydrophobic properties of the catalyst surface can be easily understood. On the one hand, hydrophilicity of the catalytic surface will favor glycerol adsorption in proximity of the active sites. On the other hand, more hydrophobic surfaces would help the removal of water produced as by-product of the reaction, locally shifting the reaction towards the formation of solketal. In fact, the elimination of water using a Dean-Stark apparatus has already proved to have a positive effect on the solketal yield.[10] As the surface of silicates is decorated by silanol groups, its hydrophilic-hydrophobic balance can be tuned by alkylation procedures using a co-synthetic or a post-synthetic approach.[28, 32] In 2006, Ji et al. reported on the synthesis of functionalized mesoporous silicates via an aerosol process but their use in catalysis was not reported.[33] Recently, we reported on aerosol-made methyl-functionalized stanno-silicates catalysts and their application in the production of ethyl lactate.[28] To the best of our knowledge, the role played by the hydrophobic/hydrophilic properties of the catalytic surface on the acetalization of glycerol to solketal was never systematically investigated.

Here, we take advantage of the aerosol-assisted sol-gel process to develop a co-synthesis approach and obtain, in a one-pot and green procedure, a novel class of alkyl-functionalized gallosilicates. The specific functionalization of the catalyst surface is presented as a way to further improve catalytic performances while taking into account the sustainability of the process.

Experimental Section

Materials

Pluronic® P-123 (Merck), Pluronic® F127 (Merck), hydrochloric acid 2M (Roth), tetraethyl orthosilicate (TEOS 97%, TCI), methyltriethoxysilane (MTES 98%, TCI), propyltriethoxysilane (PrTES 98%, TCI), phenyltriethoxysilane (PhTES 99%, TCI) and ($Ga(NO_3)_3 \cdot xH_2O$, ROTH) . Absolute ethanol (analytical grade) was supplied from Fisher Scientific.

Catalyst preparation

To synthesize functionalized Ga-silicates (Ga-P-x and Ga-F-x), a mixture of two silica sources, tetraethyl orthosilicate (TEOS) and methyltriethoxysilane (MTES) for methyl functionalized solids, propyltriethoxysilane (PrTES) for propyl functionalized solids or phenyltriethoxysilane (PhTES) for phenyl functionalized solids was prepared. In the synthesis of methyl functionalized solids, the quantity of MTES was chosen to reach three degrees of functionalization: 5, 10 and 15 %$_{mol}$, corresponding to the molar MTES / (MTES + TEOS) x 100 % ratio. For propyl and phenyl functionalized solids, the amount of PrTES or PhTES was adjusted to achieve a degree of functionalization of 5 %$_{mol}$. Pluronic F127 and P123 were selected as structure directing agents. The detailed amounts of TEOS and alkylsilane used for each material are reported in Table S1.

TEOS and MTES or PrTES or PhTES were hydrolyzed in an aqueous solution of HCl 0.02 M (20 g) to yield solution 1. Solution 2 was prepared by dissolving Pluronic® P123 or F127 (3.9 g) in absolute ethanol (45 g). Solution 1 and 2 were respectively stirred during 15 hours and 40 minutes at room temperature. Then, the gallium precursor ($Ga(NO_3)_3 \cdot xH_2O$) was added to solution 1 in order to have a Si/Ga molar ratio equal to 74. Solutions 1 and 2 were mixed together and then stirred for 30 minutes. The resulting solution was atomized with a 6-Jet 9306A atomizer from TSI. Then, the aerosol was passed through a tubular quartz tube heated at 350 °C. A cellulose nitrate filter was used to collect the powders, further dried for one night at 80 °C and calcined under static air at 250 °C for 8 h (heating rate of 1 °C/min).

Characterization

Transmission electron microscopy (TEM) images were taken using a Philips Tecnai 10 microscope operating at 80 kV. Nitrogen adsorption-desorption analyses were carried out at 77 K with a volumetric adsorption analyzer (Micromeritics ASAP 2420). Prior to the analysis, the samples were pre-treated 8 hours at 150 °C under reduced pressure (0.1 mbar). The Brunauer–Emmet–Teller (BET) method was applied in the 0.05-0.30 P/P$_0$ range to calculate the specific surface area, while the pore size distributions were calculated from the adsorption isotherm using the Barrett–Joyner–Halenda (BJH) method. The micropore volume and micropore surface area were calculated by the t-plot method that was applied to the adsorption branch of the isotherms in the thickness range of 3.5–5.0 Å. The micropore diameter was evaluated by DFT method using cylinder geometry, N_2 – Cylindrical Pores – Oxide surface model. Powder X-ray diffraction (XRD) patterns were recorded on a PANalytical X'pert diffractometer with Cu Kα radiation (k = 1.54178 Å). Inductively coupled plasma optical

emission spectroscopy was employed to determine the chemical composition of the materials using an Optima 8000 ICP-OES Spectrometer. The silicon environment and the coordination of the gallium atoms were studied by ^{29}Si Magic Angle Spinning (MAS) and ^{71}Ga MAS Nuclear Magnetic Resonance (NMR), respectively.

^{29}Si NMR spectra were recorded at room temperature on a Bruker Avance-500 spectrometer operating at 11.7 T (99.3 MHz for ^{29}Si) using a 4 mm CP-MAS Bruker probe. The sample was packed in a 4 mm zirconia rotor and measured with a spinning frequency of 8000 Hz. Quantitative direct excitation (DE-MAS) ^{29}Si spectra were recorded using the following acquisition parameters: 300s relaxation delay, 3µs (90°) excitation pulse, 52 ms acquisition time. Cross polarization (CP-MAS) spectra were recorded using a 5 s relaxation delay and 5 ms contact time. The processing comprised exponential multiplication of the FID with a line broadening factor of 30 Hz, zero-filling, Fourier transform, phase and baseline corrections. The chemical shift scale was calibrated at room temperature with respect to a sample of solid 3-(Trimethylsilyl)-1-propanesulfonic acid sodium salt (DSS) (0.0 ppm).

^{71}Ga NMR spectra were recorded at room temperature on a Bruker Avance-500 spectrometer operating at 11.7 T using a 2.5 mm CP-MAS Bruker probe. The sample was packed in a 2.5 mm zirconia rotor and measured with a spinning frequency of 25000 Hz. The spectra were recorded using a Hahn echo sequence and the following acquisition parameters: a relaxation time of 0.3 s, an excitation of 2.6 µs (90°) and 16 ms acquisition time. Data processing includes the multiplication of the FID (Free Induction Decay) by a line broadening factor of 1000 Hz, zero-filling, Fourier transformation and phase and baseline corrections. Fourier transformation from the echo maximum ensured a flat baseline with only zero-order phase correction. The chemical shift scale was calibrated at room temperature with respect to a sample of solid gallium nitrate (0.0 ppm).

Vapor-phase water adsorption isotherms were acquired at 295 K, using a surface characterization analyzer (Micromeritics 3Flex). Prior to the analysis, the sampled were pre-treated 8 hours at 180°C under reduced pressure (0.07 mbar). Water was purified using freeze-pump-thaw cycles.

Thermogravimetric analysis (TGA) were performed on a Mettler Toledo TGA/DSC 3$^+$ STARe System. The samples were analysed using a temperature ramp from 30 °C to 800 °C at 10 °C min^{-1} under air flow (60 mL min^{-1}).

FT-IR measurements were performed in transmission mode by using a Bruker Tensor 27 spectrometer equipped with a liquid nitrogen-cooled mercury–cadmium–telluride (MCT) detector, operating at a 2 cm^{-1} resolution. A pre-treatment was carried out using a standard vacuum frame, in an IR cell equipped with KBr windows. The sample was pressed into self-standing wafers and outgassed 1h at 400 °C before adsorption of ammonia at room temperature.

Adsorption of ammonia was studied in the pressure range 0.01–20.0 mbar: the reversible fraction of the adsorbed ammonia was then removed by prolonged outgassing at room temperature.

Production of solketal from glycerol and acetone

Acetalization of glycerol with acetone: glycerol (purity 99 %, 0.92 g, 0.01 mol), acetone (2.32 g, 0.04 mol) and the selected catalyst were added in a round bottom flask. The mixture was heated at 50 °C under 800 rpm stirring during a specific time. After the reaction has reached room temperature, 3 mL of absolute ethanol were added and the mixture was centrifuged (4500 rpm, 10 min). 0.5 mL of the supernatant was dried under reduce pressure and analyzed by ^{1}H-NMR, using DMSO-d6 as solvent.

Hot filtration test: glycerol (0.92 g, 0.01 mol), absolute EtOH (0.70 mL) acetone (2.32 g, 4 equiv.) and 25 mg catalyst were added in a round-bottom flask. The mixture was heated at 50 °C under 800 rpm stirring during 1 hour. The catalyst was separated from the reaction mixture by hot filtration (~ 50 °C) and centrifugation (4500 rpm, 10 min). 0.5 mL of the supernatant was dried under reduce pressure and analyzed by ^{1}H-NMR, using DMSO-d6 as solvent. The remaining amount of supernatant was kept at 50 °C for another 5 hours under 800 rpm stirring. The reaction mixture was then analyzed by ^{1}H-NMR, using DMSO-d6 as solvent.

Recycling tests: glycerol (1.56 g, 0.017 mol), acetone (4 equiv.) and the catalyst (50 mg), were added in a round-bottom flask. The mixture was heated at 50 °C under 800 rpm stirring during 1 hour. After the reaction has reached room temperature, 3 mL of absolute ethanol were added and the catalyst was separated from the mixture by centrifugation (4500 rpm, 15 min). 0.5 mL of the supernatant was dried under reduce pressure and analyzed by ^{1}H-NMR, using DMSO-d6 as solvent. Then, the supernatant was carefully removed from the centrifuge tube and the catalyst was rinsed with ethanol (3 times) and centrifuged. After this, the catalyst was calcined in air at 300 °C for 2 h (heating rate: 1 °C/min). The subsequent catalytic tests were carried out by repeating this procedure from the beginning (the quantities were adapted as a function of the mass of recovered catalyst).

Results and discussion

Two series of functionalized Ga-silicates (Si/Ga atomic ratio of 74) were prepared via a co-synthetic approach exploiting the aerosol-assisted sol-gel process and using three different alkyl-silanes: methyl, propyl and phenyltriethoxysilane. In addition, two structure-directing agents from the Pluronic family (F127 and P123) were selected in order to study their impact on the morphological properties and on the catalytic activity of the materials.

Initially, Ga-based solids were synthesized selecting three degrees of methyl-functionalization: 5, 10 and 15%$_{mol}$ (see experimental section for more information). These materials were denoted as Ga-P-x-Me and Ga-F-x-Me, where P or F indicate the employed templating agent (**P**123 or **F**127 respectively) and x indicates the nominal degree of functionalization. In order to investigate the effect of different alkyl moieties on the textural and surface properties of the solids, four additional functionalized materials were synthesized using only 5%$_{mol}$ of propyl or phenyltriethoxysilane. The materials were denoted as Ga-P(or

F)-5-Pr and Ga-P(or F)-5-Ph (where 5 indicates the degree of functionalization, Pr or Ph indicates the presence of propyl or phenyl moieties respectively). All the above-mentioned functionalized Ga-silicates were then compared to their non-functionalized analogues synthesized under the same conditions, respectively named Ga-P-0 and Ga-F-0.

After the synthesis, particular attention should be paid to preserve the alkyl-functionalization while removing the surfactant to release porosity. In the literature, several methods including solvent extraction[34] or calcination[35] have been reported to remove Pluronics from silica-based porous solids. However, taking inspiration from one of our previous work, a mild calcination treatment was here selected.[28] We found that the best compromise between a total removal of the templating agent and an almost full preservation of the functionalization can be achieved with a calcination at 250 °C for 8 hours.
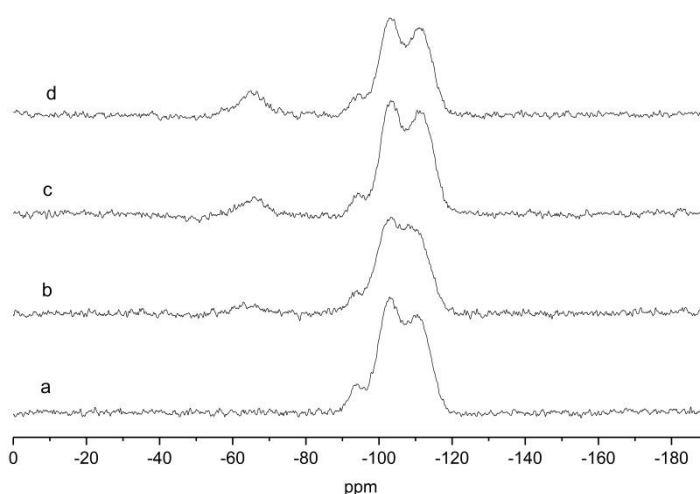
Figure 1. Solid-state direct excitation ^{29}Si MAS NMR spectra of (a) Ga-P-0 (b) Ga-P-5-Me (c) Ga-P-10-Me (d) Ga-P-15-Me after calcination at 250 °C for 8h

Thus, all the solids were calcined at the selected temperature and analyzed performing quantitative ^{29}Si solid-state magic angle spinning (MAS) NMR experiments. Figure 1 shows an example of quantitative ^{29}Si direct excitation (DE) MAS spectra of the Ga-P-x-Me series. The spectra of the other materials can be found in supporting information (Figure S1-S4). The characteristic contributions typical of an amorphous silica matrix can be observed clearly: Q^4 [(SiO)$_4$Si] (around -111 ppm), Q^3 [(SiO)$_3$SiOH] (around -102 ppm) and Q^2 [(SiO)$_2$Si(OH)$_2$] (around -92 ppm) signals can be found in all samples. Two additional signals at −66 and −59 ppm can be seen in the ^{29}Si NMR spectra of methyl-functionalized solids and can be assigned to MeSi(OSi)$_3$ (T^3) and Me(HO)Si(OSi)$_2$ (T^2) species.[28] These contributions can be found as well in the whole series of functionalized solids (see Figure S1-S4) and they attest the successful functionalization of the surface. ^{29}Si DE-MAS NMR spectra highlight also that the theoretical percentage of organic moieties is largely preserved for all material (see Table S2). These results corroborate the efficiency of the synthetic procedure including the mild calcination treatment.

The gallium loading was evaluated by inductively coupled plasma optical emission spectroscopy (ICP-OES). The experimental composition – expressed in mmol of gallium per gram of catalyst – was very close to the nominal composition of 2.2 mmol/g (Table S2) for all the solids. Nevertheless, the formation of catalytically active acid sites, fundamental for the application of these solids as catalysts, is strictly related to the insertion of Ga as single sites. The isomorphous substitution of silicon atoms by trivalent elements, as gallium, is known to induce a combination of Brønsted and Lewis acid sites within the silica framework.[21] The coordination environment of gallium was therefore elucidated via solid-state ^{71}Ga NMR spectroscopy. Due to the low gallium loading replacing silicon in an amorphous environment, the investigations were performed under magic angle spinning (MAS) at 25 kHz and at high magnetic field (11.7 T).[22]
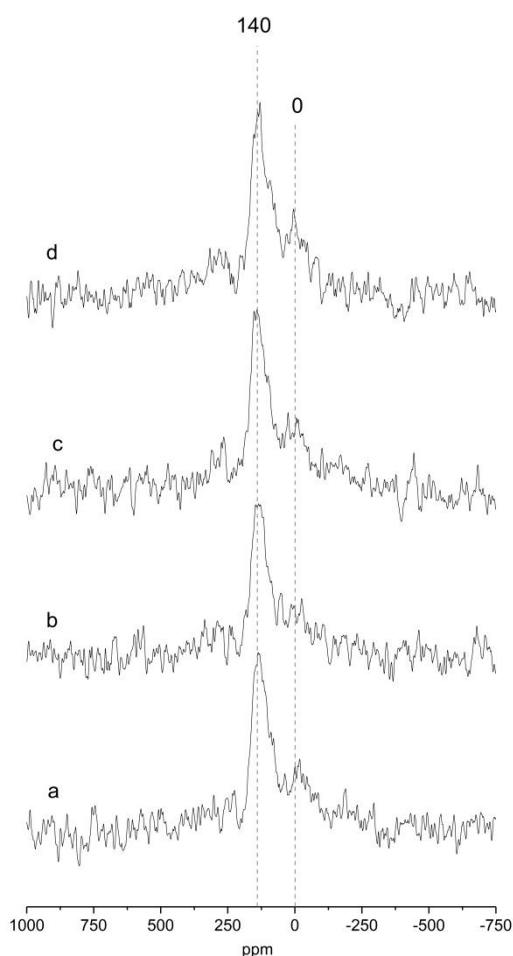
Figure 2. Solid-state ^{71}Ga MAS NMR spectra of (a) Ga-P-0 (b) Ga-P-5-Me (c) Ga-P-10-Me (d) Ga-P-15-Me after calcination at 250 °C for 8h. The spectra were recorded using a Hahn echo sequence (see experimental)

Figure 2 shows the MAS NMR spectra of Ga-P-0, Ga-P-5-Me, Ga-P-10-Me and Ga-P-15-Me. The sharp peak centered at +140 ppm, observed for all the materials, is ascribed to tetrahedral framework gallium and it constitutes a proof of the incorporation of mainly single-site Ga in the silica framework. [36, 37] This contribution has already been observed for other gallo-silicates reported in literature. The presence of an additional weak contribution at 0 ppm can be assigned to the presence of minor amounts of extra-framework Ga species (see Figure

S5 for a comparison with a pure Ga_2O_3 spectrum). These species are supposed to have an octahedral environment and have already been reported not to be catalytically active.[21] Similar results were obtained analyzing the environment of Ga in the case of Ga-F-0 (Figure S5). [71]Ga NMR measurements indicate that neither the presence of methyl-functional groups nor their amount affects the incorporation of gallium in the silica framework of the materials. It appears also that the chemical environment of gallium is not influenced by the nature of the templating agent.

The samples morphology was investigated via transmission electron microscopy (TEM). All solids are mesoporous and displays a spherical shape. The average pore diameter lies between 6 and 7 nm, typical of aerosol solids templated with Pluronic P123 or F127.[28, 38] When F127 was used as a surfactant, a well-organized structure was obtained even when the methyl-functionalization was raised up to 15% (Figure 3e to 3h). Interestingly, a slight deformation of the structure in the external part of the particles was visible for the materials synthesized in the presence of Pluronic P123 (Figure 3a to 3d). This deformation was more evident with the increasing amount of methyl-functionalization. Major modification of the structure with the appearance of some "onion like" organizations are clearly visible raising the functionalization to 15%. This behavior was previously observed and has been ascribed to the different balance among the hydrophilic part (poly(ethylene oxide)) and the hydrophobic part (poly(propylene oxide)) of the two triblock polymers.[28] As indicated by their formula, the templating agent Pluronic P123 ($(PEO)_{20}$-$(PPO)_{70}$-$(PEO)_{20}$) has a lower number of hydrophilic units than Pluronic F127 ($(PEO)_{100}$-$(PPO)_{65}$-$(PEO)_{100}$).
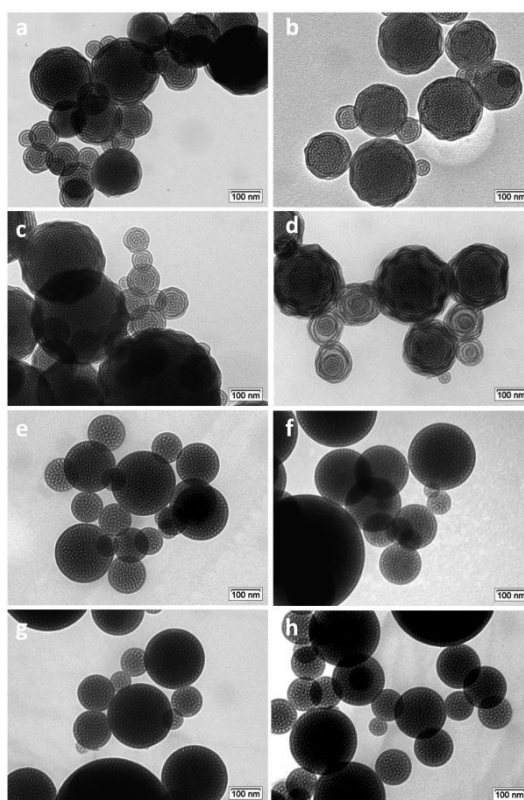
Figure 3. TEM micrographs of (a) Ga-P-0 (b) Ga-P-5-Me (c) Ga-P-10-Me (d) Ga-P-15-Me and of (e) Ga-F-0 (f) Ga-F-5-Me (g) Ga-F-10-Me (h) Ga-F-15-Me

As consequence, the methyl groups of MTES could have more affinity with the hydrophobic unit of P123 than F127. Since the methyl group of MTES is hydrophobic enough to present cosurfactant properties, it will be preferentially located nearby the hydrophobic shell of the micelle, causing a structural deformation in the final material. This behaviour may induce a variation of the interfacial curvature favouring the transition through a lamellar phase.

In the case of Ga-P-5-Pr and Ga-P-5-Ph, well-organized spherical particles were observed (Figure S6). Thus, longer organic chains as in the case of propyl moieties or bulkier phenyl groups, did not provoke a substantial deformation of the structure.

Table 1 Textural properties and composition of Ga-silicate solids

Material	BET SSA ($m^2 \cdot g^{-1}$)	BJH pore width (nm)	Pore Volume (cm^3/g)	Ga (mmol/g)[1]	% Funct.[2]
Ga-P-0	440	7.8	0.6	2.0	-
Ga-P-5-Me	410	7.1	0.6	1.9	4
Ga-P-10-Me	430	7.3	0.5	1.8	8
Ga-P-15-Me	480	6.6	0.5	1.8	13
Ga-P-5-Pr	500	7.0	0.6	1.8	< 3
Ga-P-5-Ph	460	6.6	0.5	2.0	< 3
Ga-F-0	550	7.8	0.5	2.1	-
Ga-F-5-Me	500	7.5	0.4	1.8	3
Ga-F-10-Me	460	6.9	0.4	1.9	8
Ga-F-15-Me	500	6.8	0.4	1.9	14
Ga-F-5-Pr	550	7.1	0.5	2.0	< 3
Ga-F-5-Ph	450	6.3	0.4	2.0	< 3

[1] mmol of gallium per gram of catalyst determined by ICP-OES analysis [2] % Funct. $= 100 * \left(\dfrac{T^i}{\sum_i T^i + Q^i} \right)$
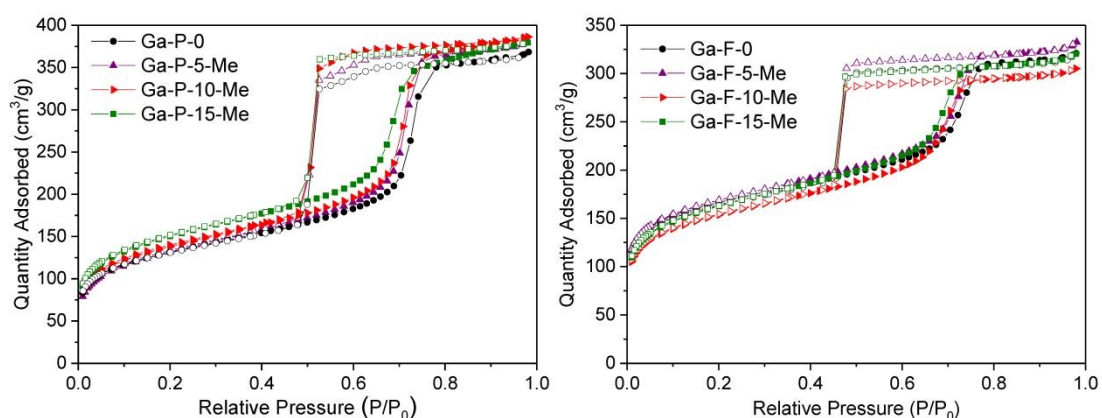
Figure 4. Nitrogen adsorption/desorption isotherms of Ga-P-0, Ga-P-5-Me, Ga-P-10-Me and Ga-P-15-Me (left) and Ga-F-0, Ga-F-5-Me, Ga-F-10-Me and Ga-F-15-Me (right) after calcination at 250 °C for 8h

The low angle powder XRD patterns of Ga-silicates templated with P123 or F127 (Figure S7) featured mainly first order d_{100} diffraction peaks, indicating well-ordered materials. The d-spacing associated to the P123 and F127 series are respectively 9 nm and 11 nm, that is typical of ordered mesostructured silicates assembled using a non-ionic surfactant. For both series, N_2-physisorption measurements showed type-IV isotherms characterized by considerable hysteresis loops. P123 templated solids present H1 hysteresis loops with steeper branches, typical of materials with narrow distribution of relatively uniform mesopores (Figure 4 and Figure S8). F127 templated materials exhibit a H2 hysteresis loop characteristic of cage-type mesopores with a mean pore diameter of 7 nm (Figure 4 and Figure S8). All solids display a high specific surface area and narrow pore size distribution. An overview of the textural properties of the two series of functionalized Ga-silicates is reported in Table 1.

The reaction selected in this work is represented by the acetalization of glycerol with acetone to produce solketal. Based on literature data, a proposed mechanism for the target reaction catalyzed by Brønsted or Lewis acid catalyst is shown in Figure S9.[19, 39] The effective insertion of single-site tetrahedral gallium, proved by solid-state [71]Ga NMR, should give rise to the desired acidic properties essentials in promoting the upgrade of glycerol into solketal.

In Table 2 the catalytic performances in the conversion of glycerol into solketal for the whole set of solids are presented. Considering sustainability as a key aspect of the process, the tests were carried out under solvent free conditions at 50 °C. A kinetic study using Ga-P-0 or Ga-F-0 as catalyst was performed (Figure S10). The formation of solketal was followed from 1 hour to 16 hours in order to select the adequate reaction time to compare the activity of our catalysts in the kinetic regime (initial activity). It appears that a short reaction time of two hours represents the best compromise between an adequate solketal yield allowing an accurate quantification and a meaningful comparison among the catalysts far enough from the equilibrium conversion.

To verify the reproducibility of the catalytic results, the materials were tested three times under the same reaction conditions. The associated error calculated was around 2% in absolute value, proving the highly reproducibility of the tests.

The comparison between functionalized and non-functionalized catalysts, synthesized under the same conditions (compare entries 1 and 7 with 2 and 8 in table 2), revealed that the 5% methylated solids Ga-P-5-Me and Ga-F-5-Me present improved catalytic activity in terms of TON (defined as moles of solketal produced per moles of Ga), even when the activity is normalized to the BET surface area (Figure S11). From this comparison emerged a positive influence of the methylation on the performances of the catalysts. It is important to underline that only a low degree of methylation allows to enhance the catalytic activity of the solids. This phenomenon was already reported by our group, in the case of functionalized Sn-silicates used in the production of ethyl lactate.[28] The observed enhancement in terms of TON could be attributed to the surface functionalization rather than to the presence of active sites (gallium single sites) in a different coordination environment. Moreover, the presence of bulkier functional groups in the formulation (see entries 5, 6 and 11, 12) leads to a lowering

of the activity. To deeply investigate this point, water vapor sorption experiments were performed at 295 K on Ga-P-0, Ga-P-5-Me, Ga-P-5-Pr and Ga-P-5-Ph (Figure S12, left). In order to meaningfully compare our solids, the amount of water adsorbed was normalized by the BET specific surface area. The quantitative evaluation of water affinity of the catalysts surface was featured at low relative pressure of the isotherm (in our case, 0.15), as indicated in the literature.[40] As illustrated in Figure S12 and Table S3 (compare entries 1 and 2), a reduced affinity for water at low relative pressure is observed for Ga-P-5-Me compared to Ga-P-0. These data suggest that the addition of methyl groups in our formulation allows to tune the hydrophilic-hydrophobic balance of our material to more hydrophobic surfaces. The less hydrophilic surface of Ga-P-5-Me may have a role in glycerol acetalization by locally helping the removal of water from the active sites and therefore favoring the formation of solketal. The quicker removal of water from the hydrophobic surface may help preserving the integrity of the acid sites of the catalyst. In comparison with Ga-P-5-Me, the water uptake at low relative pressure is lower for Ga-P-5-Pr and Ga-P-5-Ph (compare entries 2 with 3 and 4 in Table S3). This result highlights that the presence of bulkier groups in our catalysts induces more hydrophobic surfaces. Water sorption measurements evidence that the presence of too bulky hydrophobic moieties in our materials have a detrimental effect on their catalytic activity, hindering probably the adsorption of glycerol in proximity of the active sites.

Table 2 Catalytic activity of Ga-silicates in the conversion of glycerol to solketal. Conditions of the catalytic tests: 10 mg of catalyst, 50°C, 2 hours, glycerol: acetone = 1 (0.01 mol) : 4.

Entry	Material	Y_{SK} (%)	Sel.$_{SK}$ (%)[1]	TOF[2]	TON[3]
1	Ga-P-0	21	84	532	1014
2	Ga-P-5-Me	25	85	663	1326
3	Ga-P-10-Me	18	82	506	1012
4	Ga-P-15-Me	18	82	500	1000
5	Ga-P-5-Pr	17	83	462	923
6	Ga-P-5-Ph	13	79	328	656
7	Ga-F-0	10	81	242	484
8	Ga-F-5-Me	16	83	434	867
9	Ga-F-10-Me	12	82	311	622
10	Ga-F-15-Me	9	79	240	479
11	Ga-F-5-Pr	10	80	243	485
12	Ga-F-5-Ph	9	77	224	447

[1] Sel.$_{SK}$ = mol solketal / (mol solketal + mol 2,2-Dimethyl-1,3-dioxan-5-ol). The presence of the by-product (2,2-Dimethyl-1,3-dioxan-5-ol) was identified via ^{1}H liquid state NMR (Figure S13) [2]TOF (TurnOver Frequency) here defined as mol of solketal/mol of Ga * time. [3]TON (TurnOver Number) here defined as mol of solketal/mol of Ga after 2 hours of reaction.

No further improvement in the catalyst performance was observed when the methylation degree is brought to 10% (see entries 3 and 9) or to 15% (see entries 4 and 10). To go further, the series of Ga-P-x methylated materials were analyzed via thermogravimetric analysis (TGA). In order to evaluate the hydrophobic/hydrophilic nature of our solids, the weight loss was quantified at 140°C and normalized by the BET specific surface area. As illustrated in Figure S12 (right), when the percentage of methyl moieties increases, the desorption of physiosorbed water decreases. These results indicate that an enhancement of the percentage of methylation allows achieving a more hydrophobic surface. All these results confirm that the fine tuning of the hydrophilic-hydrophobic balance of the catalytic surface play a crucial role in the design of more active catalysts.

Surprisingly the solids synthesized employing P123 as surfactants display predominantly better catalytic performances than the corresponding materials of the F127 series (compare entries 1 to 6 with 7 to 12). Considering the ^{71}Ga MAS NMR analysis, the insertion of Ga as single site is very similar on Ga-P-0 and Ga-F-0 (Figure S5). Their textural properties deserve therefore an in-depth characterization to better understand the observed inequalities in terms of catalytic activity.

It is well-known that the presence of micropores in heterogeneous catalysts can limit the diffusion of reagents to the active sites and/or the release of the products from the active sites. The presence of micropores in the walls of Ga-P-0 and Ga-F-0 was here evaluated via the t-plot method. In the case of Pluronic templated solids, the formation of micropores occurs by aggregation of the hydrophilic blocks of two micelles within the pre-formed silica walls. This phenomenon leads to microporosity in the final material once the templated agents are eliminated via calcination.[41] The analysis of the t-plot allows accessing to the microporous area and micropore volume of our solids (Figure S14). The microporous surface area of Ga-F-0 and Ga-P-0 amounts to 250 m^2/g and 170 m^2/g, respectively. Ga-F-0 and Ga-P-0 display micropore volumes of 0.08 cm^3/g and 0.04 cm^3/g, respectively. The analysis via the mathematical modeling using density functional theory (DFT) allows evaluating the diameter of the micropores that is located in the 1 to 2 nm range. Hence, the decreased activity of the Ga-F-0 could be at least partially ascribed to a limited accessibility of the active sites located in the micropores.

However, to shed more light on the different catalytic behavior, FT-IR measurements of ammonia adsorption on Ga-P-0 and Ga-F-0 solids were conducted as well. This analysis allows investigating the acidic properties and providing a support for an interpretation to the observed catalytic performances. For this study, ammonia (a basic molecular probe), which can interact both with Brønsted (surface hydroxyls) and Lewis (unsaturated Ga (III)) sites was selected.
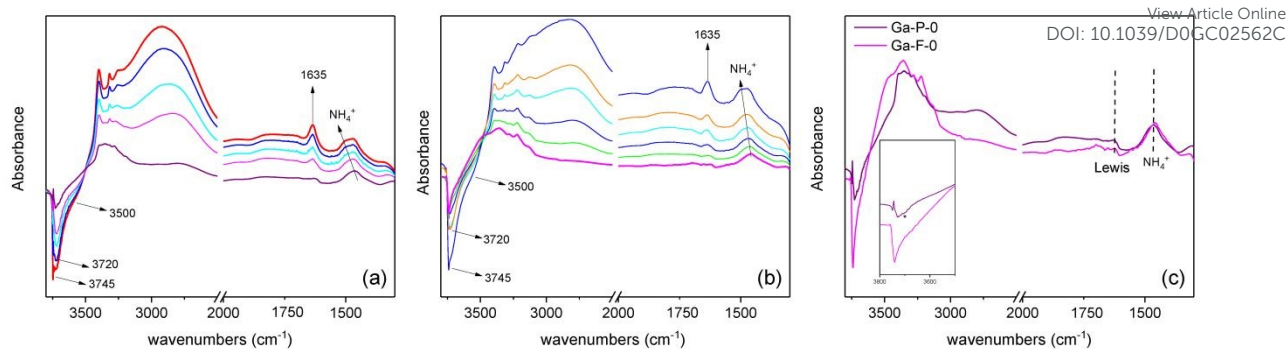
Figure 5. Difference FT-IR spectra of NH$_3$ dosages on (a) Ga-P-0, (b) Ga-F-0 and (c) outgassed at room temperature

FT-IR difference spectra of ammonia adsorption on both Ga-P-0 and Ga-F-0 are shown in Figure 5 (a and b), where the negative bands indicate species that disappear upon ammonia dosages. In the high frequency region (3800-2000 cm^{-1}), the adsorption of ammonia generates the formation of several negative bands due to the various hydroxyls interacting with NH$_3$. In particular, both samples show a negative band at about 3745 cm^{-1} due to free silanols and two negative bands at about 3720 cm^{-1} together with a broad shoulder at 3550 cm^{-1} related to terminal and H-bonded silanols in hydroxyls chains, respectively.[42] The positive signal at around 3400 and 3316 cm^{-1} are ascribed to N-H stretching modes and the broad envelope in the high frequency range is due to the hydroxyl species engaged in H-bonding with ammonia molecules.

In the low frequency region (1800-1300 cm^{-1}), for both samples the absorption band at 1635 cm^{-1} corresponds to the bending mode of NH$_3$ molecules H-bonded to surface OH groups, whereas the broad signal at around 1460 cm^{-1} is due to the bending mode of NH$_4^+$ ions formed by proton-transfer reaction from Brønsted sites. The formation of ammonium ions on both solids indicates that the incorporation of Ga within the silica framework provides Brønsted sites that are enough acidic to protonate NH$_3$, at variance with surface hydroxyls of unsubstituted mesoporous silica which only establish hydrogen-bonding. The blue shift of the ammonium band observed with increasing NH$_3$ equilibrium pressure is generally ascribed to the multiple lateral interactions of NH$_4^+$ ions with surface oxygen atoms and/or OH groups. As expected from ^{71}Ga NMR both Ga-F-0 and Ga-P-0 display similar acid properties. However, a direct comparison between the difference spectra of Ga-P-0 and Ga-F-0 outgassed at room temperature after ammonia dosage (Figure 5c) allow evidencing some differences. It is important to highlight that the observed residual signals correspond to species formed on the strongest acidic sites and thus irreversible upon ammonia removal. In the high frequency region, the fully outgassed samples show some dissimilarities, in particular for Ga-P-0 the residual broad signal at around 2800 cm^{-1} is more intense than that found on Ga-F-0, suggesting a larger population of residual H-bonded silanols in interaction with ammonia. Furthermore, a close inspection of the residual negative hydroxyl bands of the two samples evidences more intense residual free silanols band (3744 cm^{-1}) for Ga-F-0 compared to Ga-P-0, which at variance shows higher negative components at 3720 cm^{-1} and at 3500 cm^{-1}. Moreover, a negative shoulder at about 3692 cm^{-1} (labelled with an asterisk in the inset) can

be discerned on Ga-P-0, which based on the literature can be ascribed to hydroxyl linked to gallium sites, in analogy to that is observed on hydroxylated gallium oxide.[43]

For both fully outgassed samples the signal of NH_4^+ ions became less intense upon outgassing (reversible proton transfer) and for the two samples a very similar residual intensity can be claimed. The absorption band attributed to NH_3 physisorbed on silanols (1635 cm^{-1}) decreased in intensity and was red-shifted up to 1621 cm^{-1} for the fully outgassed samples (residual pressure $< 1.10^{-3}$) ascribed to ammonia molecules adsorbed on Ga^{3+} acting as Lewis sites, in analogy to amorphous aluminosilicates.[42] Since this signal appears slightly more intense for Ga-P-0 than for Ga-F-0, it can be assumed as an evidence of a little higher concentration of exposed surface Lewis sites.

Taken together, these spectroscopic data reveal very similar surface features in term of acidic sites for the two samples. However, some differences regarding the hydroxyl populations and Lewis site concentration have been evidenced, suggesting an overall higher acidity of Ga-P-0 surface, most likely due to a Ga-enriched surface compared to Ga-F-0. This slightly higher acidity of Ga-P-0 solid together with the increased accessibility of the active sites (lower contribution of micropores) may constitute a synergistic combination of features contributing to the enhanced catalytic performances.
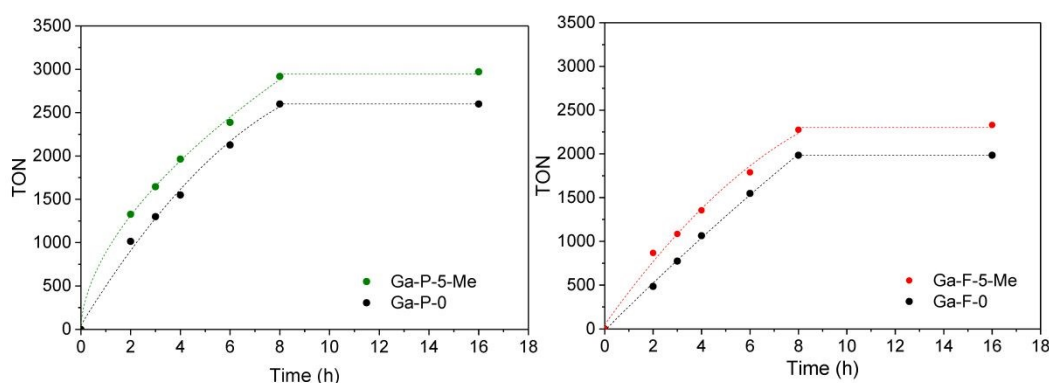
Figure 6. Evaluation of the catalytic activity over time. Comparison between Ga-P-5-Me and Ga-P-0 (left), Ga-F-5-Me and Ga-F-0 (right). Conditions of the catalytic tests: 10 mg of catalyst, 50°C, glycerol: acetone = 1 (0.01 mol): 4
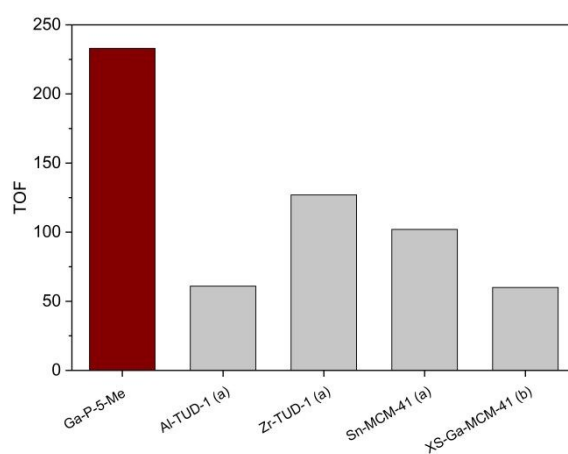
Figure 7. Comparison of the catalytic activity of Ga-P-5-Me with metal-containing silicates reported in literature for the conversion of glycerol to solketal: (a)[19], (b)[21]. Conditions of the catalytic test: 25 mg of catalyst, 1.48 g of tert-butanol, 80°C, 2 hours, glycerol: acetone = 1 (0.01 mol): 4.

The catalytic activity of the best materials in each series was also evaluated over time (Figure 6). Regardless of the catalyst considered, the TON increased rapidly during the first 8h of reaction followed by a plateau (the conversion values at 8h are reported in Table S4). The functionalized materials display a higher TON compared to non-functionalized materials. Moreover, the difference observed between non-functionalized and functionalized materials remains constant over time.

In order to have a meaningful notion of the performances of our best catalyst (Ga-P-5-Me), an additional catalytic test was performed in the presence of t-butanol, a solvent commonly used in the literature to convert glycerol into solketal. The comparison with reference materials illustrated in Figure 7 evidence the outstanding catalytic performances of Ga-P-5-Me. The high activity of our solid can be ascribed to a combination of aspects such as the incorporation of gallium mainly as single site, its open mesostructure or even the functionalization of its surface with low amount of methyl groups.

In the perspective of sustainable processes promoted by heterogeneous catalysts, a pivotal role is played by the robustness of the catalyst under the selected reaction conditions, which determines the possibility to reuse it in multiple catalytic runs. The reusability of our most promising catalyst – Ga-P-5-Me – was evaluated in consecutive cycles (Figure 8, left). At the end of each cycle, the catalyst was recovered by centrifugation, washed with ethanol and thermally regenerated at 300°C for two hours. It is important to highlight that the selected thermal treatment allows to preserve the initial amount of methyl groups in our catalyst as confirmed by quantitative ^{29}Si MAS measurement (Figure S14). The calcination treatment is of fundamental importance since it was already reported that the activity gradually decreases upon reuse if the catalyst is only washed with solvent. From this study emerged that the good activity and selectivity of the catalyst was preserved at least for four catalytic cycles.

In order to investigate the stability of Ga-P-5-Me, a hot filtration experiment was performed as well (Figure 8, right). The solketal yield was measured after one hour of reaction after which the catalyst was removed by hot filtration (50 °C). The filtrate was then reacted for 5 additional hours. The hot filtration experiment shows that the solketal yield remains constant indicating the absence of active species in the filtrate.
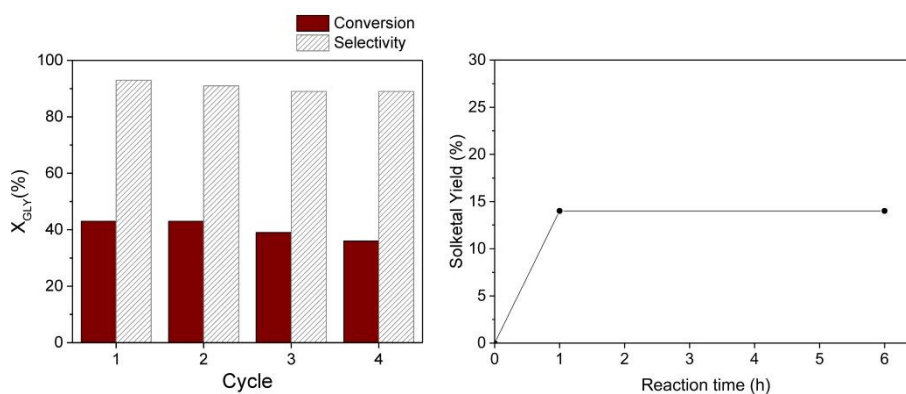
Figure 8. Recycling test with Ga-P-5-Me (left). Conditions: 50 mg of catalyst, 50°C, 1 hour, glycerol: acetone = 1 (0.017 mol): 4. Hot filtration experiment with Ga-P-5-Me (right). Conditions: 25 mg of catalyst, 0.70 mL of ethanol, 50°C, 1 hour, glycerol: acetone = 1 (0.01 mol): 4.

To further evaluate the sustainability of our process, the associated E-Factor was calculated, selecting a reaction time of 8 hours (to reach maximum conversion). After reaction, the catalyst was removed by centrifugation and acetone was recovered by distillation. The E-Factor was calculated according the following formula: E-Factor = [$(4.60\ g\ Glycerol + 11.6\ g\ Acetone - 2.41\ g\ Acetone\ recovered\ by\ distillation - 3.50\ g\ Solketal)$ $/3,50\ g\ Solketal$] = 2.9. Such low E-factor value is in the same range as typical values reported for the industrial production of bulk chemicals,[44] and support the idea that this catalytic process is promising. Moreover, the optimization of the distillation setup used to recover acetone could certainly allow further improving the E-Factor of the process.

As mentioned at the beginning of this work, the importance of preserving the organic functionalities on the surface of the solids while removing efficiently the structuring agent determined the adoption of a mild thermal treatment at 250 °C. However, in the literature, analogous non-functionalized metal-silicates are usually subjected directly to a thermal treatment ranging from 500 °C to 600 °C to effectively remove the templating agent.[21, 45, 46] It is important to highlight that the calcination temperature may affect also the physicochemical properties of the materials (e.g. surface area), but also the surface hydroxyl content, responsible of the hydrophilic character of the surface.

For this reason, we investigated the catalytic behavior of Ga-P-0 at different calcination temperatures. As reported in Figure 9, the increase of the calcination temperature from 250 °C to 550 °C had a beneficial impact on the catalytic performance of the non-functionalized solid. If we compare the physico-chemical properties of the material calcined at 250 °C and 550 °C, a decrease of the BET surface area (from 440 m^2/g to 350 m^2/g) is observed and could be ascribed to the increasing condensation of neighboring silanols (*vide infra*). The loss of BET surface area with the increase of the calcination temperature (until 550 °C) appears incoherent with the improvement of the catalytic activity. In fact, if the TON is normalized by the surface area (Figure S15), this improvement is even more evident. No other major differences were observed in terms of pore size distribution or gallium insertion (Figure S16). Therefore, these observations could be ascribed to the beneficial role played by the calcination temperature on the modification of the surface hydrophobicity.

As the temperature of the thermal treatment increases, the silica surface is dehydrated causing the removal of the adsorbed water and thermal dehydration reaction, where two adjacent silanols condense into a siloxane bridge. Experimental data reported in the literature demonstrated that increasing the temperature of the thermal treatment the silica surface becomes more hydrophobic due to the condensation of surface hydroxyls and the formation of siloxane bridges.[47-49] The reduction of the hydroxyl groups population, was here proved by the higher degree of condensation. The latter was estimated by deconvolution analysis using Gaussian functions of the ^nQ contributions on quantitative direct excitation ^{29}Si MAS NMR spectra (Figure 10). This last procedure could represent an interesting alternative to modify

the hydrophilic/hydrophobic balance of the surface proving again its beneficial role in particular on the selected reaction.

Finally, raising the calcination temperature to 650 °C resulted in a rather remarkable loss of catalytic activity that in this case could be ascribed to a major loss of surface area (around 200 m²/g), probably caused by the collapse of the catalyst structure.
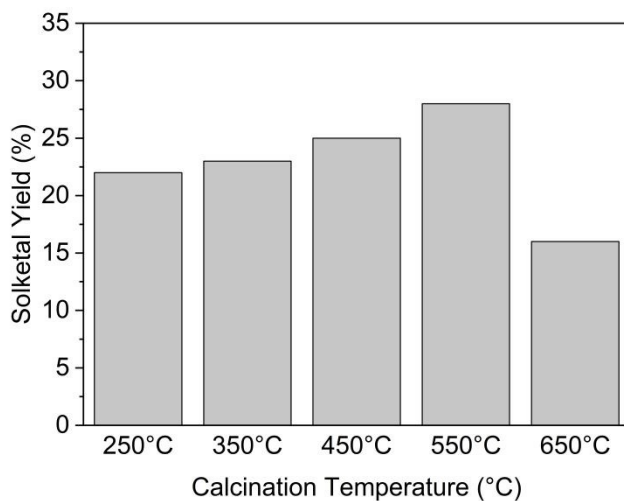
Figure 9. Study of the influence of the calcination temperature on the catalytic activity of Ga-P-0. Conditions of the catalytic tests: 10 mg of catalyst, 50°C, 2 hours, glycerol: acetone = 1 (0.01 mol): 4.
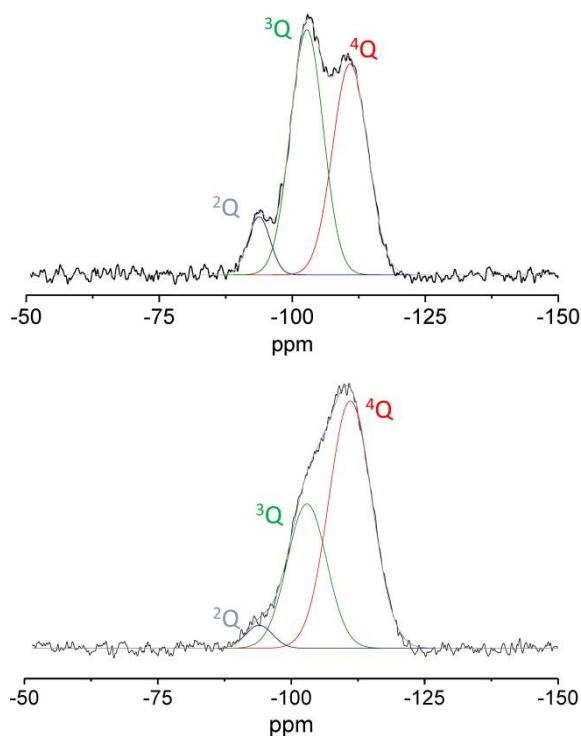
Figure 10. ^{29}Si direct excitation MAS NMR spectra of Ga-P-0 calcined at 250 °C (top) and 550 °C (bottom)

Conclusions

The aerosol process was used to synthesized, in a straightforward one-pot procedure and with low environmental impact, a series of functionalized Ga-silicates. The efficient incorporation of isolated gallium as single site within the silica framework was confirmed via ^{71}Ga solid state NMR and the stability of the organic moieties has been assessed using ^{29}Si solid-state MAS NMR. The materials exhibited record activity in the acetalization of glycerol to yield solketal at low temperature and under solventless conditions. In particular, the materials synthesized using P123 as templating agent demonstrated the best catalytic activity. A positive influence of the functionalization on the catalytic performances of the materials emerged in presence of methyl moieties. In addition, it was observed that only low degree of methylation was effective to enhance the catalytic performance of the materials, shifting locally the reaction to the production of solketal. The best catalyst was successfully used in multiple catalytic runs thus proving its robustness under the selected reaction conditions. To further evaluate the sustainability of our process, the associated E-Factor was calculated and can be compared with the E-Factor reported for the industrial production of bulk chemicals. Moreover, a systematic study evidenced the importance of a careful tuning of surface polarity, achievable not only with surface functionalization but also with different thermal treatments applied to non-functionalized solids. The control of the hydroxyl group population on the surface, possible with a control on the calcination temperature, also allowed enhancing the catalytic activity thus further supporting the pivotal role of the surface polarity. Nevertheless, considering the balance between sustainability and performances as a key aspect, functionalized solids constitute the best option as they present the advantage of a less energy-consuming thermal treatment at mild temperature.

Conflicts of interest

There are no conflicts of interest to declare.

Acknowledgements

References

1. Transforming our world: the 2030 Agenda for Sustainable Development, https://sustainabledevelopment.un.org/post2015/transformingourworld#, (accessed 06/05/2020).
2. A European Green Deal, https://ec.europa.eu/info/strategy/priorities-2019-2024/european-green-deal_en, (accessed 06/05/2020).
3. Renewable Energy – Recast to 2030 (RED II), https://ec.europa.eu/jrc/en/jec/renewable-energy-recast-2030-red-ii, (accessed 06/05/2020).
4. I. M. Atadashi, M. K. Aroua and A. A. Aziz, *Renewable and Sustainable Energy Reviews*, 2010, **14**, 1999-2008.
5. T. Issariyakul and A. K. Dalai, *Renewable and Sustainable Energy Reviews*, 2014, **31**, 446-471.
6. M. Pagliaro, R. Ciriminna, H. Kimura, M. Rossi and C. Della Pina, *Angewandte Chemie International Edition*, 2007, **46**, 4434-4440.
7. P. T. Anastas and J. C. Warner, *12 Principles of Green Chemistry. Green Chemistry: Theory and Practice*, Oxford Univ. Press New York, 1998.
8. A. Behr, J. Eilting, K. Irawadi, J. Leschinski and F. Lindner, *Green Chemistry*, 2008, **10**, 13-30.
9. J. I. García, H. García-Marín and E. Pires, *Green Chemistry*, 2014, **16**, 1007-1033.
10. M. R. Nanda, Y. Zhang, Z. Yuan, W. Qin, H. S. Ghaziaskar and C. Xu, *Renewable and Sustainable Energy Reviews*, 2016, **56**, 1022-1031.
11. A. Cornejo, I. Barrio, M. Campoy, J. Lázaro and B. Navarrete, *Renewable and Sustainable Energy Reviews*, 2017, **79**, 1400-1413.
12. R. A. Sheldon, *ACS Sustainable Chemistry & Engineering*, 2018, **6**, 32-48.
13. T. N. Pham, T. Sooknoi, S. P. Crossley and D. E. Resasco, *ACS Catalysis*, 2013, **3**, 2456-2473.
14. F. D. L. Menezes, M. D. O. Guimaraes and M. J. da Silva, *Industrial & Engineering Chemistry Research*, 2013, **52**, 16709-16713.
15. R. Gérardy, D. P. Debecker, J. Estager, P. Luis and J.-C. M. Monbaliu, *Chemical Reviews*, 2020, DOI: 10.1021/acs.chemrev.9b00846.
16. L. Roldán, R. Mallada, J. M. Fraile, J. A. Mayoral and M. Menéndez, *Asia-Pacific Journal of Chemical Engineering*, 2009, **4**, 279-284.
17. P. Ferreira, I. M. Fonseca, A. M. Ramos, J. Vital and J. E. Castanheiro, *Applied Catalysis B: Environmental*, 2010, **98**, 94-99.
18. J. Kowalska-Kus, A. Held, M. Frankowski and K. Nowinska, *Journal of Molecular Catalysis A: Chemical*, 2017, **426**, 205-212.
19. L. Li, T. I. Korányi, B. F. Sels and P. P. Pescarmona, *Green Chemistry*, 2012, **14**, 1611-1619.
20. G. Vicente, J. A. Melero, G. Morales, M. Paniagua and E. Martín, *Green Chemistry*, 2010, **12**, 899-907.
21. X. Collard, L. Li, W. Lueangchaichaweng, A. Bertrand, C. Aprile and P. P. Pescarmona, *Catalysis Today*, 2014, **235**, 184-192.
22. A. Vivian, L. Soumoy, L. Fusaro, P. Louette, A. Felten, S. Fiorilli, D. P. Debecker and C. Aprile, *Synthesis and In-Depth Characterization of Ga-Based Structured Catalysts: Enhancing Glycerol Conversion*, 2020, *ChemRxiv*, doi: 10.26434/chemrxiv.12612926.v1
23. D. P. Debecker, S. Le Bras, C. Boissière, A. Chaumonnot and C. Sanchez, *Chemical Society Reviews*, 2018, **47**, 4112-4155.
24. C. Wang and H. Bai, *Industrial & Engineering Chemistry Research*, 2011, **50**, 3842-3848.
25. L. Kuai, J. Geng, C. Chen, E. Kan, Y. Liu, Q. Wang and B. Geng, *Angewandte Chemie International Edition*, 2014, **53**, 7547-7551.
26. V. Smeets, C. Boissière, C. Sanchez, E. M. Gaigneaux, E. Peeters, B. F. Sels, M. Dusselier and D. P. Debecker, *Chemistry of Materials*, 2019, **31**, 1610-1619.
27. E. Kan, L. Kuai, W. Wang and B. Geng, *Chemistry – A European Journal*, 2015, **21**, 13291-13296.

28. A. Vivian, L. Fusaro, D. P. Debecker and C. Aprile, *ACS Sustainable Chemistry & Engineering*, 2018, **6**, 14095-14103.
29. F. Colbeau-Justin, C. Boissière, A. Chaumonnot, A. Bonduelle and C. Sanchez, *Advanced Functional Materials*, 2014, **24**, 233-239.
30. D. P. Debecker, M. Stoyanova, F. Colbeau-Justin, U. Rodemerck, C. Boissière, E. M. Gaigneaux and C. Sanchez, *Angewandte Chemie International Edition*, 2012, **51**, 2129-2131.
31. A. Kim, C. Sanchez, B. Haye, C. Boissière, C. Sassoye and D. P. Debecker, *ACS Applied Nano Materials*, 2019, **2**, 3220-3230.
32. V. Smeets, L. Ben Mustapha, J. Schnee, E. M. Gaigneaux and D. P. Debecker, *Molecular Catalysis*, 2018, **452**, 123-128.
33. X. Ji, Q. Hu, J. E. Hampsey, X. Qiu, L. Gao, J. He and Y. Lu, *Chemistry of Materials*, 2006, **18**, 2265-2274.
34. M. Kruk, M. Jaroniec, C. H. Ko and R. Ryoo, *Chemistry of materials*, 2000, **12**, 1961-1968.
35. R. M. Grudzien and M. Jaroniec, *Chemical Communications*, 2005, 1076-1078.
36. C. R. Bayense, A. P. Kentgens, J. W. De Haan, L. J. Van de Ven and J. H. Van Hooff, *The Journal of Physical Chemistry*, 1992, **96**, 775-782.
37. M. Chatterjee, T. Iwasaki, Y. Onodera, T. Nagase, H. Hayashi and T. Ebina, *Chemistry of Materials*, 2000, **12**, 1654-1659.
38. N. Godard, A. Vivian, L. Fusaro, L. Cannavicci, C. Aprile and D. P. Debecker, *ChemCatChem*, 2017, **9**, 2211-2218.
39. M. R. Nanda, Z. Yuan, W. Qin, H. S. Ghaziaskar, M.-A. Poirier and C. C. Xu, *Fuel*, 2014, **117**, 470-477.
40. D. H. Olson, W. O. Haag and W. S. Borghard, *Microporous and Mesoporous Materials*, 2000, **35-36**, 435-446.
41. W. J. J. Stevens, K. Lebeau, M. Mertens, G. Van Tendeloo, P. Cool and E. F. Vansant, *The Journal of Physical Chemistry B*, 2006, **110**, 9183-9187.
42. B. Bonelli, B. Onida, J. D. Chen, A. Galarneau, F. Di Renzo, F. Fajula and E. Garrone, *Microporous and Mesoporous Materials*, 2004, **67**, 95-106.
43. C. Otero Areán, A. L. Bellan, M. P. Mentruit, M. R. g. Delgado and G. T. Palomino, *Microporous and Mesoporous Materials*, 2000, **40**, 35-42.
44. R. A. Sheldon, *Green Chemistry*, 2017, **19**, 18-43.
45. R. Luque, J. M. Campelo, T. D. Conesa, D. Luna, J. M. Marinas and A. A. Romero, *Microporous and mesoporous materials*, 2007, **103**, 333-340.
46. K. Okumura, K. Nishigaki and M. Niwa, *Microporous and Mesoporous Materials*, 2001, **44-45**, 509-516.
47. V. Bolis, B. Fubini, L. Marchese, G. Martra and D. Costa, *Journal of the Chemical Society, Faraday Transactions*, 1991, **87**, 497-505.
48. E. F. Vansant, P. Van Der Voort and K. C. Vrancken, *Characterization and chemical modification of the silica surface*, Elsevier, 1995.
49. A. Matsumoto, T. Sasaki, N. Nishimiya and K. Tsutsumi, *Colloids and Surfaces A: Physicochemical and Engineering Aspects*, 2002, **203**, 185-193.